ACS APPLIED BIO MATERIALS

www.acsabm.org Article

Ultrahigh Penetration and Retention of Graphene Quantum Dot Mesoporous Silica Nanohybrids for Image Guided Tumor Regression

Rajendra Prasad,*,# Nishant K. Jain,# Amit S. Yadav, Manali Jadhav, Nalukurthi Naga Venkata Radharani, Mahadeo Gorain, Gopal C. Kundu, João Conde,* and Rohit Srivastava*

Cite This: *ACS Appl. Bio Mater.* 2021, 4, 1693−1703 Read Online

ACCESS | Metrics & More | Article Recommendations | Supporting Information

ABSTRACT: So far, near-infrared (NIR) light responsive nanostructures have been well-defined in cancer nanomedicine. However, poor penetration and retention in tumors are the limiting factors. Here, we report the ultrahigh penetration and retention of carbanosilica (graphene quantum dots, GQDs embedded mesoporous silica) in solid tumors. After NIR light exposure, quick (0.5 h) emission from the tumor area is observed that is further retained up to a week (tested up to 10 days) with a single dose administration of nanohybrids. Emissive and photothermally active GQDs and porous silica shell (about 31% drug loading) make carbanosilica a promising nanotheranostic agent exhibiting 68.75% tumor shrinking compared to without NIR light exposure (34.48%). Generated heat (~52 °C) alters the permeability of tumor enhancing the accumulation of nanotheranostics into the tumor environment. Successive tumor imaging ensures the prolonged follow-up of image guided tumor regression due to synergistic therapeutic effect of nanohybrids.

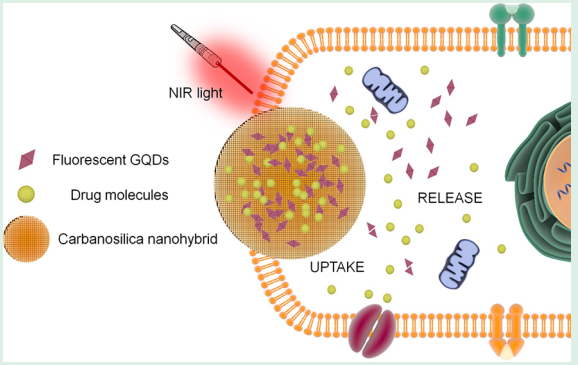

KEYWORDS: *graphene quantum dots, porous silica, solid tumor, photothermal therapy, nanotheranostic, tumor regression*

INTRODUCTION

From past decades, the rapid progress in developing near-infrared (NIR) light responsive nanostructures and their phototriggered strategies has been noticed.[1−9] Further, nanodiagnostics and nanotherapeutics hold much promise for the precise diagnosis and treatment of tumors.[1,10−25] Moreover, only a few smart nanomaterials have progressed for clinical applications.[26−41] Among them, gold−silica,[26] liposome−doxorubicin,[30,31] and organic dyes[40] are very popular for targeted imaging and phototriggered therapy in human trials.[28−31,33,35,37−40] However, deep penetration with prolonged retention in tumor is a remaining challenge of attempted nanohybrids.[29−32] Apart from the above systems, porous silica (especially, mesoporous silica, MS),[18,42] macrocyclic assemblies,[43−45] and carbon based materials[46−48] have gained much attention for biomedical, bioimaging, or sensing and catalysis applications.[49] Interestingly, MS is recognized as a safe biomaterial for drug delivery applications due to their high surface area, large cargo capacity, and biocompatibility.[50−53] Nevertheless, their low targeting ability, poor accumulation in tumors and slow degradation are being questioned.[50−56] Therefore, to overcome these limitations, biodegradable nanohybrids have been proposed recently but they are far from addressing the site-selective tumor imaging and image guided tumor regression.[57−59] On the other hand, fluorescent graphene quantum dots (GQDs) have been widely used for tumor diagnosis and near-infrared (NIR) light responsive photothermal therapy in cancer nanomedicine.[60−66] These GQDs are highly promising for targeted tumor imaging due to their ultrasmall size, deep tissue visualization, and high aqueous dispersibility. However, the rapid clearance of GQDs is a critical issue so far.[60,61,63] Overall, MS and fluorescent GQDs have been recognized as promising platforms for diagnostics and cancer therapeutics individually.[54−65] Next, GQDs integrated mesoporous silica (MS) is a recent development for cancer diagnostics and therapeutics.[18,63−65] Especially, carbon nanodots incorporated mesoporous silica is recently reported for photothermal-immunotherapy but far from explaining about the image guided tumor regression with a precise follow-up.[67]

In terms of cancer therapeutics strategies, standalone photothermal, photodynamic therapy, chemotherapy, and radiation therapy are widely explored but unable to eliminate the solid tumor.[10,18−21] Consequently, the synergistic or combinational therapeutics such as chemo-photothermal, chemo-photodynamic, and photothermal−photodynamic have

Received: November 12, 2020
Accepted: January 4, 2021
Published: January 8, 2021

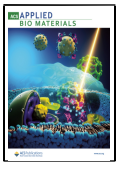

https://dx.doi.org/10.1021/acsabm.0c01478
ACS Appl. Bio Mater. 2021, 4, 1693−1703

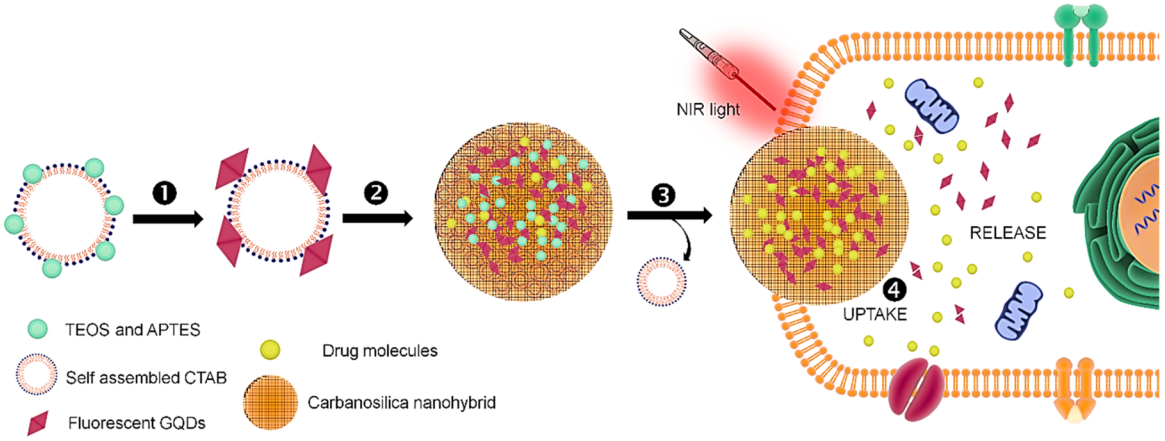

Figure 1. Schematic showing the surfactant mediated sol−gel process of red fluorescent graphene quantum dots encapsulated porous silica nanohybrids named as carbanosilica. Deposition of silica precursor (a mixture of (3-aminopropyl)triethoxysilane (APTES) and tetraethylorthosilicate (TEOS)) on self-assembled CTAB surfactant ①, decoration of red emissive graphene quantum dots on silica coated CTAB assemblies ②, matured fluorescent graphene quantum dots encapsulated porous silica nanohybrids ③, and surfactant free fluorescent graphene quantum dots encapsulated porous silica nanohybrids uptake into cancer cells during NIR light exposure ④.

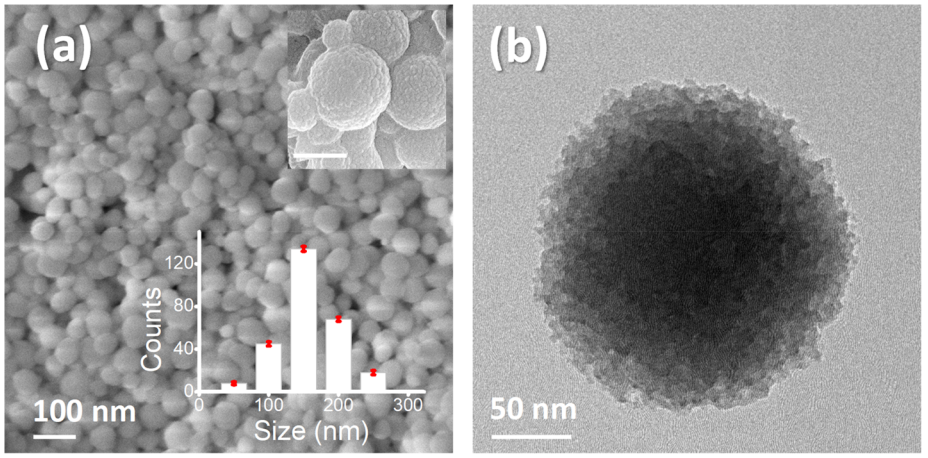

Figure 2. Scanning electron microscopic (SEM, a) and transmission electron microscopic (TEM, b) images of carbanosilica (graphene quantum dots (GQDs) embedded mesoporous silica). Inset shows the particle size distribution of carbanosilica nanoparticles.

been recently conceptualized for tumor ablation.[24,60,61,64,65,68−70] However, these treatment strategies are in the developing phase and face the consequences of slow tumor growth inhibition.[61,65]

Here, the interaction between designed carbanosilica (graphene quantum dots, GQDs embedded mesoporous silica) and solid tumor environment has been examined under nonionized light irradiation (800 nm). The rapid accumulation (0.5 h) with strong retention of fabricated nanohybrids is achieved with a single dose administration. Further, the synergistic therapeutic effect of nanohybrids exhibited about 68.75% tumor shrinking compared to without NIR light exposure (34.48%). Moreover, a precise follow-up of image guided tumor regression has been demonstrated successfully. Overall, the present work provides a new direction for safe diagnosis and advanced cancer therapy for solid tumor elimination.

RESULTS AND DISCUSSION

Fluorescent graphene quantum dots (GQDs) embedded mesoporous silica (carbanosilica) nanohybrids are achieved through a surfactant mediated sol−gel process[18] that is tested for tumor penetration and image guided tumor regression under near-infrared (NIR, a nonionized light) light irradiation (see Figure 1). Prior to designing carbanosilica, emissive GQDs are prepared from *Mangifera indica* (mango) leaves through a microwave-assisted route by following an earlier reported procedure with some modifications.[66] The physicochemical properties of these prepared GQDs are tested by using various characterization techniques. Transmission electron microscopic (TEM) imaging measurements demonstrate the uniform size distribution of synthesized GQDs (about 7 nm in size) as shown in Figure S1a−c.

In absorption spectra, the observed broad peak around 400 nm indicates the unsaturated carbonic framework in synthesized GQDs that further appears between 500 and 900 nm exhibiting the presence of surface functional groups and a conjugated carbon network (see Figure S1d). Additionally, dilution dependent (0.0125−2.5 μg/mL) aqueous dispersion tests demonstrate the better dispersion and stability of these prepared GQDs even after 24 h of incubation time (see Figure S1e). Overall, the microscopic and spectroscopic analysis ensured the physicochemical stability of the GQDs that makes them suitable for biomedical applications. Further, these GQDs are embedded/or encapsulated in the silica shell (named as

https://dx.doi.org/10.1021/acsabm.0c01478
ACS Appl. Bio Mater. 2021, 4, 1693−1703

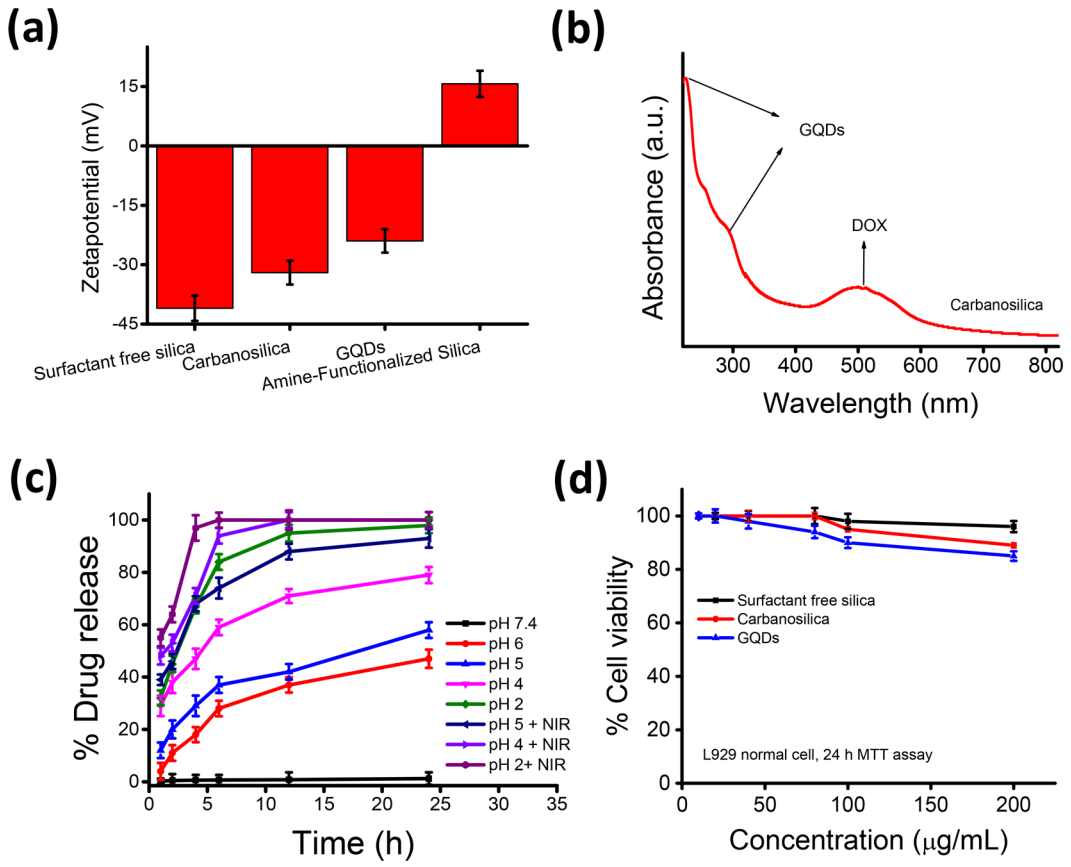

Figure 3. Surface charge measurements (zeta potential) of carbanosilica, surfactant free silica, amine functionalized silica, and GQDs (a). Absorption spectrum of doxorubicin drug loaded carbanosilica (b). % Drug release performance of engineered nanohybrids at various cellular conditions before and after NIR light irradiation (c). % Cell viability of carbanosilica, surfactant free silica, and GQDs measured by MTT assay at various concentrations (d). $n = 3$ is considered to measure mean and standard deviation.

carbanosilica) via base catalyzed hydrolysis and condensation of silica and aminated silica precursors. The condensation at higher temperature results in the formation of silica particles encapsulated with GQDs that is thoroughly washed with Milli-Q and methanol. Porous frameworks of designed carbanosilica are achieved via an acid leaching procedure. The shape and morphology of synthesized carbanosilica nanoparticles are confirmed through scanning and transmission electron microscopic images (SEM and TEM, about 120−140 nm size) as shown in Figure 2a,b. The effective distribution of GQDs in the silica framework is clearly noticed through microscopic images (see Figure S1f−j). The even distribution of GQDs in the versatile silica network is due to electrostatic interaction between the anionic surface of quantum dots and amino groups of the silica network (confirmed through surface charge analysis as discussed below). The morphology and particle size distribution of engineered carbanosilica nanohybrids (GQDs embedded porous silica) are similar to mesoporous silica nanoparticles (100−130 nm in size) where clear porous architecture is evaluated through transmission electron microscopic images (see Figure S1h). Moreover, the exterior surface roughness of carbanosilica nanoparticles is analyzed through scanning electron microscopy (SEM) indicating the decoration of GQDs in the silica framework as shown in Figure 2a and Figure S1i,j. Remarkably, the time dependent colloidal stability of the resulting nanoparticles is tested in different solutions, viz., PBS, cell culture medium, and serum. These prepared samples have been analyzed through dynamic light scattering (DLS) and digital photographs at different time points (0 h to 12 days). DLS exhibits about 260−300 nm diameter of carbanosilica with better polydispersity index (PDI, 0.85). Further, these observations are corroborated with digital photographics measurements showing good dispersion even after 12 days of test indicating better colloid stability of designed carbanosilica (see Figure S1k,l in the Supporting Information).

Further, the hexagonal ordered porous[18] network (100 plane at 2θ angles 2.66°) in carbanosilica is observed through the X-ray diffraction pattern that is slightly different from parent mesoporous silica nanohybrids/surfactant free silica (empty silica nanoparticles, 100 plane at 2θ angles 2.47°, see Figure S2a). The major shift in the 100 plane indicates the encapsulation of GQDs in silica nanohybrids that is further substantiated with elemental analysis (energy dispersive X-ray analysis, EDAX) as shown in Figure S2b. The elemental peak of Si, N, C, and O indicates the amino functionalized silica network and ensures the encapsulation of GQDs in silica particles. The N_2 adsorption−desorption isotherm of engineered carbanosilica nanohybrids demonstrates high surface area (about 850 m^2/g) with a pore volume of 0.39 cm^3/g whereas surfactant free silica nanoparticles demonstrate larger surface area (1000 m^2/g) with 0.98 cm^3/g pore volume (see Figure S2c). The drastic variation in surface area and pore volume confirms the encapsulation of GQDs in the silica network (named as carbanosilica) that is corroborated with microscopic measurements. Interestingly, the ordered porous network and high surface area of designed carbanosilica make them versatile materials for high drug

https://dx.doi.org/10.1021/acsabm.0c01478
ACS Appl. Bio Mater. 2021, 4, 1693−1703

loading and controlled drug delivery applications as shown in Figure S2d.

The surface charge of GQDs and designed nanohybrids (0.5 mg/mL in aqueous suspension) is analyzed through zeta potential measurement as shown in Figure 3a. Due to the presence of hydroxyl functional groups, negative zeta potentials are measured for GQDs (−24 mV) and surfactant free silica (−41 mV) nanoparticles whereas positive zeta potential (15.7 mV) is observed for amine functionalized porous silica indicating the successful functionalization with amino silane linkers. On the other hand, carbanosilica exhibits a moderate negative zeta potential (−32 mV) as compared to parent silica nanoparticles indicating the encapsulation of negatively charged GQDs within the amine functionalized silica framework and the strong electrostatic interaction between hydroxyl functional groups of quantum dots and amine functional groups of silica networks. After removing the surfactant from the carbanosilica nanohybrids, anticancer drug is loaded for further cancer therapeutic applications. The encapsulation of GQDs and drug molecules is further confirmed through absorption spectroscopic analysis showing the peaks between 220 and 310 nm (C═C and C═O) and a broad absorption in the NIR region (700−1000 nm) indicating the presence of hydrophilic functional groups and unsaturated carbonic frameworks in GQDs (see Figure 3b). Additionally, a broad peak between 490 and 500 nm ensures the presence of doxorubicin hydrochloride anticancer drug (∼31% loading capacity, see Figure S2d and eq S5). The stimuli-triggered drug release performance of DOX loaded carbanosilica is examined in physiological (pH 7.4) and tumor mimicked (pH 2, 4, 5, 6 and pH 2, 4, 5 in under NIR exposure) conditions. A negligible drug release (about 1.5%) is observed in physiological conditions (pH 7.4 at 37 °C) whereas more than 50% drug release is measured in the cancer mimicked environment (pH 2−5) during a 24 h incubation period (see Figure 3c). At pH 6, the designed nanohybrid demonstrates about 47% drug release performance whereas more than 90% drug release is noticed in the late endosomal environment (pH 2) due to the potential effect of H^+ ions. Slow drug release (about 58% in 24 h) is observed in the case of pH 5 that is further improved (about 93%) after NIR light exposure due to the effect of generated heat. On the other hand, in 24 h of incubation, about 79% drug release is observed at pH 4 that further increased to about 99.5% under NIR light exposure under the same conditions (pH 4 and 800 nm NIR exposure for 5 min) whereas NIR irradiated late endosomal condition (pH 2 under NIR exposure) exhibits about 100% drug release within 6 h of incubation due to the impact of generated photothermal heat and high potential of H^+ ions.

Prior to imaging and therapeutic validations (at *in vitro* and *in vivo* level), the emissive nature of the designed carbanosilica is confirmed through photoluminescence spectroscopy at different excitations (530 and 620 nm) showing emission in the range of 665 to 730 nm due to the entrapped GQDs within the porous silica network (see Figure S3a and the high resolution TEM image shown in Figure S1i,j). The red emission from designed nanohybrids may be due to the conjugated framework,[60,61,66] surface defects, and functional groups of encapsulated GQDs in carbanosilica that help in localized tumor diagnosis and observation of image guided tumor shrinking. Due to an effective GQD entrapment and broad absorption in the NIR region, the carbanosilica demonstrates higher photothermal transduction (about 55 °C within 5 min) with continuous exposure of NIR radiation (1 W/cm^2 of 800 nm wavelength, see Figure S3b−d). The photothermal performance of carbanosilica nanohybrids is validated at 0.5 and 1 mg/mL, showing a constant rise in temperature in a nanohybrid concentration and laser exposure time dependent way by stabilizing initial temperature at 37 °C. Interestingly, hyperthermia temperature (43 °C) is achieved in less than 2 min of NIR light irradiation, which is adequate for cell membrane disruption.[56,61,66] Measured 47.9 °C temperature (considered as ablation temperature) within 3 min of NIR exposure is sufficient to begin the ablation of tumor cells (surfactant free silica and phosphate-buffered saline, PBS, are considered as controls). Recently, plasmonic gold nanoshell has been tested clinically for localized photothermal ablation of prostate tumors using 4.5 W/cm^2 to 6.5 W/cm^2 of laser power. However, high power of laser may cause inflammation and rashes on the irradiated area. To avoid the aforementioned issues, 1 W/cm^2 power of NIR laser has been widely practiced.[26,71−73]

Here, we have applied 1 W/cm^2 of laser for therapeutic validations due to the better penetration ability of exposed laser. The designed carbanosilica structures (0.5 mg/mL of 100 μL) have been tested to evaluate the photothermal conversion efficiency (about 42%) using ON-OFF cycles during NIR light irradiation. We have noticed the steady temperature rise during repeated cycles demonstrating better photothermal stability of designed nanohybrids where steady-state temperature and the cooling temperatures are recorded by an IR digital thermometer (Figure S3c,d and eqs S1−S4). Each component of the carbanosilica nanohybrids, such as GQDs and surfactant free silica are found to have better biocompatibility measured through MTT assay (see Figure 3d). *In vitro* MTT assay of emissive GQDs, surfactant free silica, and carbanosilica was carried out on fibroblastic L929 normal mouse adipose tissue cell line at various concentrations (10−200 μg/mL). More than 85% cell viability is observed at the highest concentration of carbanosilica nanohybrids (200 μg/mL) demonstrating their significant biocompatibility, making them suitable for *in vivo* studies. The biocompatibility of carbanosilica nanohybrids is compared with its components such as GQDs and surfactant free silica exhibiting about 85% and about 96% biocompatibility at 200 μg/mL concentration respectively whereas almost 100% cell viabilities are observed at 20 μg/mL.

Figure 4 shows the therapeutic capacity of the carbanosilica nanohybrid (200 μg/mL) measurements accessed on breast cancer 4T1[60,61] cell line before and after NIR exposure (5 min exposure of 800 nm laser with 1 W/cm^2 power density). Doxorubicin anticancer drug loaded carbanosilica nanohybrids (200 μg/mL of concentration) present an impactful synergistic therapeutic response (about 89% cell death) under NIR light exposure (5 min) as compared to drug free carbanosilica (200 μg/mL, ∼71% cell death) and surfactant free silica (200 μg/mL, only 5% cell death). These results clearly demonstrate the development of an efficiently engineered carbanosilica nanohybrid for advanced photothermal and combinational cancer therapeutics. Prior to NIR exposure, 200 μg/mL of drug loaded carbanosilica nanohybrids show a higher cell death (about 64%), when compared to drug free carbanosilica (only 15% cell death) showing the potential performance of NIR triggered chemotherapy on breast cancer cells. Control groups such as surfactant free silica (200 μg/mL) and only NIR light demonstrate more than 95% cell viability exhibiting a nontoxic effect of silica-based nanohybrids. Additionally, cellular internalization of carbanosilica (200 μg/mL) into 4T1 breast cancer cells is examined via cell imaging studies (see Figure S4). A notable red fluorescence

https://dx.doi.org/10.1021/acsabm.0c01478
ACS Appl. Bio Mater. 2021, 4, 1693−1703

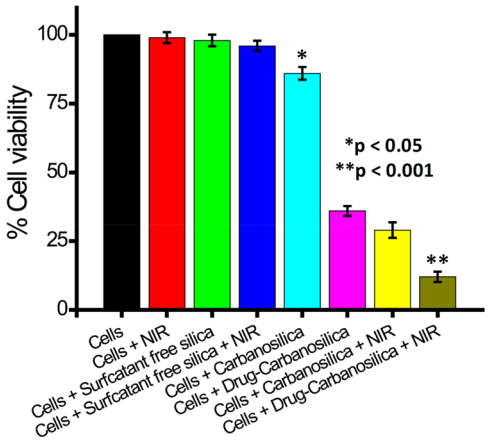

Figure 4. *In vitro* therapeutic efficacy of carbanosilica and its components (200 μg/mL of each) in 4T1 breast cancer cell lines at various conditions. Three independent sets of experiments are conducted to measure mean, standard deviation, and p values, *p < 0.05, **p < 0.001.

is observed in the cytoplasm of cancer cells within 6 h of incubation time, due to the emissive nature of encapsulated GQDs in carbanosilica, which indicates the successful uptake of the nanohybrids.

Based on the *in vitro* performances, the designed carbanosilica nanohybrids (20 mg dose) are further tested for image guided tumor regression (see Figure 5). The homogeneous and deep distribution of postinjected carbanosilica (20 mg dose) in solid tumors promotes the ablation of the cancer cells and provides detailed information on the localized tumor microenvironment due to the momentous photothermal response and red emissive nature of injected nanohybrids. GQDs with ultrasmall size and high dispersion ability provide imaging of ablated tumors with promising emission intensity during NIR light irradiation, followed by an efficient and prolonged (for days) accumulation in cancer cells.

Successive and precise follow-up of tumor regression is measured by localized tumor diagnosis, which demonstrates the impact of the synergistic phototriggered chemotherapy. A progressive reduction in tumor size/volume is measured by near-infrared fluorescence (NIRF)[61] using an *in vivo* imaging system (530 nm of excitation light). Figure 5a shows the time dependent (0.5 h to 10th day) consecutive measurements of NIR light treatment (with 800 nm laser 1 W/cm^2) and the effect on tumor shrinking in breast tumor bearing mice (female Balb/c mice after intratumoral injection of 20 mg emissive carbanosilica nanohybrids). The follow-up of NIRF imaging of tumor after NIR exposure exhibits (1) promising tumor regression after NIR light irradiation with a single dose of nanohybrid; (2) localized tumor imaging; and (3) prolonged retention/accumulation ability (tested up to 10 days) (see Figure 5a and 5b). Maximum fluorescence intensity (about 10 × 10^7 p/cm^2/sr) from the postinjected tumor area is observed after 1 h post NIR treatment indicating an improved accumulation of emissive carbanosilica nanohybrids in the deep tumor environment, which is further notable up to the 10th day (about 1.89 × 10^7 p/cm^2/sr) even without injecting a second dose of carbanosilica (Figure 5b). Further, NIRF imaging demonstrates a consistent reduction in tumor size, measured through localized tumor diagnosis (81.1% reduction in fluorescent intensity) due to the generated heat (more than 47 °C) by the accumulated GQDs in the tumors. Additionally, a time dependent (0.5 h to 10th day) photo-

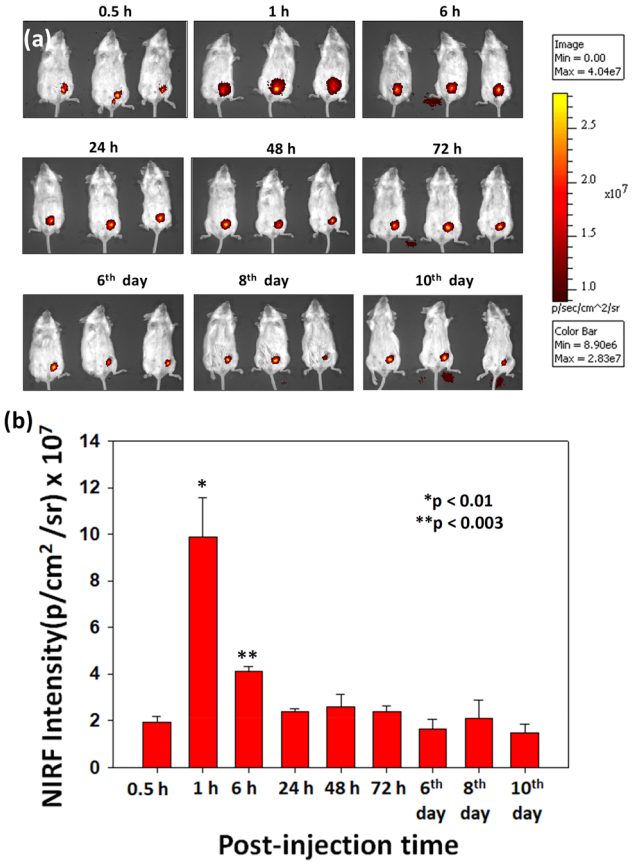

Figure 5. Follow-up (0.5 h to 10th day) of image guided tumor regression using synergistic phototriggered chemotherapy and localized tumor diagnosis after accumulation of carbanosilica (20 mg dose) as theranostic agent in the tumor microenvironment. Qualitative (a) and quantitative *in vivo* analysis (b), n = 3 is considered to measure mean, standard deviation, and p values, *p < 0.01, **p < 0.003.

thermal response (up to 55 °C) from tumor area is noticed with 5 min of NIR light exposure on postinjected tumor area, due to the presence of photothermally active carbanosilica in the tumor microenvironment (Figure S5a, b).

On the other hand, three groups (n = 5) of tumor bearing mice are prepared to evaluate the NIR light mediated synergistic phototriggered chemotherapy approach. Preinjected mice are considered as controls (group 1), with postinjection of drug loaded carbanosilica (20 mg of single dose) without NIR treatment (group 2) and postinjection of drug loaded carbanosilica (20 mg of single dose) with 5 min of NIR treatment (800 nm, group 3) being the other groups. A 20 mg single dose of drug loaded carbanosilica is injected to the 4T1 tumors (intratumoral injection). The tumor volumes are measured on each therapeutic day. Figure 6a–f demonstrates the NIR light mediated tumor regression compared to control (preinjected animal group) and chemotherapeutic groups (doxorubicin loaded carbanosilica injected without NIR exposure). Figure 6a shows significant tumor size and volume regression (320 mm^3 to 100 mm^3 at day 18) for NIR treated mice due to the synergistic photochemotherapeutic approach (see Figure S6a, b). However, only a 140 mm^3 (from 320 mm^3 to 180 mm^3) tumor size reduction is observed for mice without NIR light treatment (considered as chemotherapeutics group, postinjected doxorubicin loaded carbanosilica). Hence, the designed carbanosilica nanohybrids are capable of an improved

https://dx.doi.org/10.1021/acsabm.0c01478
ACS Appl. Bio Mater. 2021, 4, 1693−1703

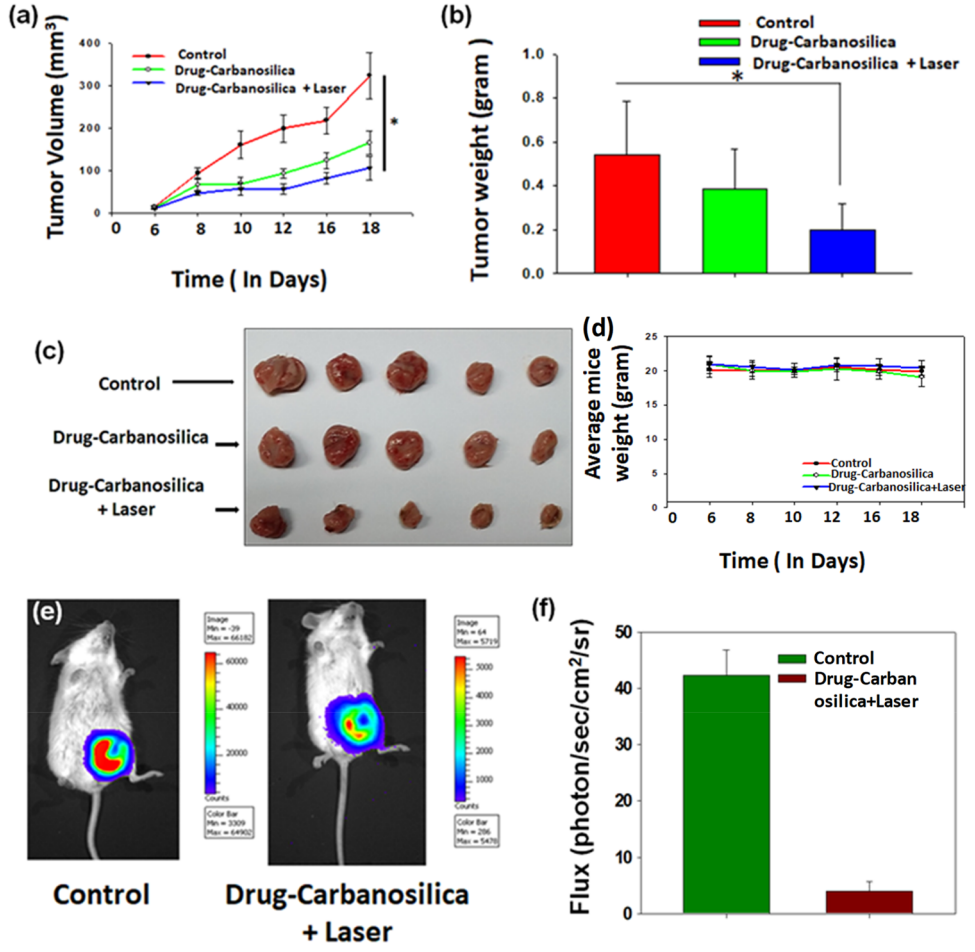

Figure 6. Measurements of image guided tumor regression and the effect of synergistic phototriggered chemotherapy on tumor volume and weight. Tumor volumes are measured using Vernier Calipers, analyzed statistically and represented graphically (n = 5) and compared with tumor bearing preinjected mice (a). After treatment, tumors are excised, weighed, and analyzed statistically, n = 5 (b). Digital photograph of collected tumor sizes during the therapeutic course, n = 5 (c, preinjected animals as control, drug loaded carbanosilica injected mice without NIR light exposure, and drug loaded carbanosilica injected mice after NIR light irradiation, 20 mg dose for each). Observation of body weight during treatment planning, n = 5 (d). Qualitative and quantitative analysis of phototriggered tumor regression using drug loaded carbanosilica injected mice after NIR light irradiation measured through *in vivo* bioluminescence imaging (e, f).

light-to-heat response during NIR light exposure, demonstrating a substantial effect on tumor ablation, confirmed through histopathological examination of NIR treated tumors (see Figure S6c). Tumor necrosis and suppressed invasion of cells are clearly noticed from histopathological analysis of carbanosilica injected tumor area after NIR light irradiation. The observed tumor necrosis after NIR exposure indicates the effect of phototriggered chemotherapy whereas lower necrosis is noticed for groups with drug loaded carbanosilica without NIR treatment due to the effect of the released anticancer drug. Nevertheless, the preinjected tumor area is observed without any necrotic county. Further, these variations are validated by measuring the tumor weight (in grams) after sacrificing the animals at day 18 (6 days after first treatment, see Figure 6b). A 0.2 g tumor weight is measured in the case of phototriggered combinatorial therapy, which is significantly lower than chemotherapeutics tumor weight (about 0.4 g) and control tumor weight (0.58 g) groups.

Overall, the extensive reduction in tumor volume and weight is due to the combined effect of generated heat and released anticancer drug during NIR light irradiation at the tumor site (see digital photographs in Figure 6c). The maintained body weight (about 20 g) and normal body score of all treated animals (n = 5 in each group) demonstrates an efficient and biocompatible carbanosilica nanotheranostics agent, associated with no toxicity effect on major organs (see Figure 6d, Figure S6b and Figure S7). Moreover, the tumor regression during phototriggered combination therapy is analyzed by *in vivo* bioluminescence measurements showing a lower intensity of 4T1 cells after NIR light responsive photothermal-chemotherapy treatment, when compared to the control (pretreated mice) as shown in Figure 6e, f.

For *in vivo* toxicity measurements, a regular animal health and body score is observed, with no injury and/or histopathological changes in vital organs (heart, lung, liver, spleen, stomach, and kidney) for all postinjected and preinjected (control) animals (Figure S8). Normal myofibers and muscle bundles are noticed in the histopathology examinations[53] of heart tissue collected from treated and control animal groups. Maintained bronchiole with epithelial linings, connective tissues and cartilage, and controlled alveoli are observed from histopathology analysis of lungs. Normal portal triad and hepatocytes are clearly noticed in the liver. No changes in white and red pulps are seen in spleen. Similarly, pits and glands are normally found in histology of the

https://dx.doi.org/10.1021/acsabm.0c01478
ACS Appl. Bio Mater. 2021, 4, 1693−1703

stomach. Additionally, parietal cells and chief cells are observed with maintained morphology. Glomeruli and tubules in kidney are also normal in all groups of mice (preinjected mice as control, drug loaded carbanosilica treated animals without NIR exposure and after NIR irradiation). Notably, Qian et al. have reported the biodegradation of silica based nanohybrids via swelling and weakening of the strong Si−O−Si network formed after polymerization of silanol condensation.[67] They have observed Si−C bond weakening by absorbing aqueous media that help in gradual degradation of the nanostructures enhanced by encapsulated quantum dots. Hence, maintained body weight, good health of treated animals, no acute changes in tissues, etc. ensure the biocompatibility of designed emissive carbanosilica nanohybrids.

KEY IMPORTANCE AND NOVELTY OF CARBANOSILICA

So far, various multifunctional organic, inorganic and biological nanohybrids have been attempted for tumor imaging and tumor ablations applications (see Table S1). However, poor penetration and retention in tumor microenvironment, toxicity, multiple and heavy dose administrations, high powered NIR light irradiation (2−6 W/cm^2), and rapid clearance are critical concerns. Apart from these limitations, sophisticated synthesis and bioengineering of nanohybrid "theranostics agents" are other major challenges. Moreover, the image guided tumor shrinking and its follow up using minimum and single dose administration of nanotheranostics have not yet been well explored. Here, in this work, we have investigated the comprehensive follow up (up to 10 days) of solid tumor shrinking/reduction upon moderate power of NIR light (1 W/cm^2) with single dose of nanohybrid (20 mg) due to better photothermal response (about 52 °C) of injected carbanosilica (graphene quantum dots, GQDs embedded mesoporous silica). Effective distribution of GQDs in porous silica network ensures the significant light to heat response. Recently, a carbon nanodots incorporated silica framework has been tested for *in vivo* antitumor therapy.[67] However, the earlier report is far from addressing high surface area (more than 700 m^2/g) that yields low cargo capacity (for an anticancer drug molecules) materials and the privation of combination chemo-photothermal therapeutic ability of synthesized nanoplatforms. Additionally, previously reported carbon nanodots-mesoporous silica nanohybrids[67] have been achieved via electrostatic assembly strategy (hydrogen bonding) that hampers the colloidal stability, porosity, and uniform distribution of designed nanohybrids, but biodegradation is a major achievement so far. In the present work, we report high surface about 850 m^2/g with a pore volume of 0.39 cm^3/g that shows about 31% of drug loading capacity due to the ordered 2D porous architecture of designed carbanosilica. Further, red emissive nature, significant photothermal response, and high cargo capacity improve the image guided combination therapeutic ability of engineered carbanosilica upon single wavelength NIR light irradiation. Importantly, high penetration and retention of injected carbanosilica in a solid tumor environment have been noticed due to phototriggered release of uniformly distributed quantum dots that is validated through *in vivo* studies. Moreover, better performance with multifunctionality at lower dose make carbanosilica a potential onconanomedicine for localized solid tumor imaging and selective tumor ablation. Overall, a cost-effective nanohybrid has been designed for image guided cancer therapy that reduces the cost of diagnosis and treatment and could give a new hope for affordable diagnosis and treatments.

CONCLUSIONS

Here, we have investigated the accumulation of emissive nanohybrids into solid tumors, which are able to persist for a long time in the tumor microenvironment. These up taken nanohybrids maintain their emissive and photothermal properties for a long time that ensures the image guided tumor regression followed by a synergistic phototriggered chemotherapy in breast cancer. Prior to *in vivo* examinations, uniform particle size distribution, deep encapsulation of graphene quantum dots in porous silica, improved stability, high surface area (850 m^2/g), and drug loading capacity (31%) are validated through physicochemical characterizations. A high photothermal response (about 48 °C in 3 min) and cargo capacity of the designed carbanosilica nanohybrids make them ideal for synergistic phototriggered chemotherapy. A single dose administration of fluorescent carbanosilica demonstrates a promising temperature rise (about 55 °C) and fluorescent intensity (10×10^7 p/cm^2/sr), which are sufficient for tumor ablation (about 68.75%) and successive follow-ups of tumor imaging. The generated heat enhances the accumulation of the silica nanohybrids into solid tumors, inducing the thermolysis of tumor cells and, therefore, promoting tumor size reduction. Moreover, a systematic observation of tumor imaging after each therapeutic trial reveals the persistent tumor regression, which is validated through several qualitative and quantitative *in vivo* analyses. Tumor regression and *in vivo* biocompatibility are substantiated with histopathological examinations. Importantly, the injected functional nanohybrids are biocompatible as confirmed through body weight and normal animal health observations. In summary, the deep tumor localization and regression clearly demonstrate the advancement of the designed carbanosilica nanohybrids as powerful nanotheranostic agents for localized tumor imaging/diagnosis and therapy.

METHODS

Materials and Characterization Techniques. *N*-Cetyltrimethylammonium bromides (CTAB, 95%), (3-aminopropyl) triethoxysilane (APTES, 98%), tetraethylorthosilicate (TEOS, 99.9%), doxorubicin hydrochloride (DOX, 96%), sodium hydroxide (98%), and (3-(4,5-dimethylthiazol-2-yl)-2,5-diphenyltetrazolium bromide-MTT) were purchased from Sigma-Aldrich. Dulbecco's Modified Eagle Medium (DMEM), Fetal bovine serum (FBS), and 4′,6-diamidino-2-phenylindole (DAPI) were obtained from HiMedia Pvt. Ltd., India. GQDs were prepared from *Mangifera indica*. Hydrochloric acid (95%), dimethyl sulfoxide (DMSO), and methanol were purchased from Merck.

Microscopic studies were demonstrated by using transmission electron microscopy (TEM), Philips CM200, and scanning electron microscopy, FEI, Model Quanta 200. Powder XRD (PXRD) patterns were recorded using a dual goniometer diffractometer with 0.4 × 12 mm line/point of focus size and Scintillator NaI, Dtex detector. Elemental analysis was done by using transmission electron microscopy. Further, UV−vis spectroscopy was performed at a path length of 1 cm using PerkinElmer Lamda-25. Adsorption−desorption isotherms using N_2 were recorded using a Quanta chrome Quadra Win instrument. Surface area was calculated using the multiple-point Brunauer−Emmett−Teller (BET) theory. Pore volume was estimated at a relative pressure of P/P_0 = 0.9. Fluorescence spectroscopy measurement was conducted using a Shimadzu instrument at a slit width of 5 nm (excitation and emission). Fluorescence microscopy was carried out by using 465-95, 540-25, and 540-80 nm filters from an inverted fluorescent microscope. *In vivo* emissive images were recorded

https://dx.doi.org/10.1021/acsabm.0c01478
ACS Appl. Bio Mater. 2021, 4, 1693−1703

using an IVIS spectrum imaging system (IVIS spectrum Xenogen). NIR light mediated photothermal transduction experiments were performed by using an 800 nm NIR laser source.

Preparation of Fluorescent Graphene Quantum Dots (GQDs). Emissive GQDs were prepared by using *Mangifera indica* (mango) leaves. The synthesis recipe was adopted from an earlier reported process with some modifications.[66] About 3 cm pieces of mango leaves were immersed in the 20 mL of ethanolic solution for 16 h. The obtained extract from leaves was collected via centrifugation (13 k rpm for three times) and further filtered multiple times. Finally, ethanol solvent was evaporated using a rotary evaporator and further processed in a hot-air oven to make concentrated product. The aqueous suspension of obtained material was treated in microwave conditions for 10 min (800 W). After completing the reaction, the prepared scum was dispersed in ethanol, was filtered, and was further dried at 70 °C to obtain graphene quantum dots (GQDs).

Synthesis of Emissive GQDs Embedded Porous Silica Nanohybrid (Carbanosilica). *N*-Cetyltrimethylammonium bromides (CTAB, 0.5 g) were dissolved in 380 mL of Millipore water under vigorous stirring at constant 85 °C temperature. After stabilizing the reaction temperature, 1.5 mL of aqueous NaOH was added to adjust the pH around 10.4. After controlling all parameters, a mixture of TEOS:APTES (400 μL from 4:1 ratio) was added dropwise into CTAB assembled aqueous suspension. After 15 min of stirring, red emissive GQDs (0.5 mg/mL) were added into the above mixture followed by control addition. A greenish milky suspension was observed after 3 h of reaction time indicating the complete hydrolysis and condensation of added silica precursors over GQDs attached CTAB assemblies. The obtained mixture was kept for 12 h without any disturbance, and then the product was collected via centrifugation (8000 rpm three times). The obtained product was thoroughly washed with the diluted methanol and further dried at 70 °C using a vacuum oven for overnight. CTAB surfactant was removed from as synthesized nanoparticles to create the porosity in fabricated nanohybrids. CTAB surfactant was removed by mixing 500 mg of as prepared nanoparticles in acidic methanol (50 mL) at 65 °C temperature followed by vigorous stirring. The final product was collected via centrifugation and washed with the methanol and dried at 70 °C using a vacuum oven. The prepared materials were characterized and used for cancer theranostics applications.

Synthesis of Doxorubicin Loaded Carbanosilica Nanohybrids. Doxorubicin hydrochloride[18] was used as a model drug to evaluate the loading capacity and therapeutics efficacy of designed carbanosilica nanohybrid. One mg/mL of doxorubicin hydrochloride was prepared in PBS (pH 7.4) that was incubated for 24 h with 200 mg of surfactant free carbanosilica nanohybrids. After complete incubation, the product was collected via centrifugation and washed with Millipore water until observing almost transparent supernatant. The mass of drug loaded in nanoparticles was calculated by subtracting the mass of drug in the supernatant from the total mass of drug used (see eq S5).

Photothermal Transduction Assessment. Photothermal transduction experiments were performed at two concentrations (0.5 and 1 mg/mL) of designed carbanosilica nanohybrid using 1 W/cm^2 power of 800 nm NIR laser source. Prior to beginning the NIR light exposed photothermal transduction, the temperature of the water bath was stabilized to 37 °C. Now, 200 μL of carbanosilica nanoparticles at two different concentrations was added into 96 well plates and exposed to 800 nm a continuous wave NIR laser source for 5 min. Time dependent photothermal response was recorded by a digital thermometer. PBS and parent surfactant free silica particles were used as controls. Further, photothermal efficiency (η) was determined by measuring the time dependent heating and cooling temperature rate of NIR treated carbanosilica nanohybrids (see Supporting Information and eqs S1−S4 for more details).

Stimuli Triggered Drug Release. To evaluate the stimuli responsive drug release pattern with respect to cancer mimicked conditions and NIR light mediated therapy, 1 mL of doxorubicin hydrochloride loaded carbanosilica nanohybrids was added in a dialysis bag that was immersed in 250 mL of PBS at various pH values (2, 4, 5, 6, and 7.4) and pH 2, 4, 5 with 800 nm NIR light irradiation for 5 min. At various time intervals, 2 mL of solution was collected and replaced with the same volume of fresh PBS solution. The obtained suspension was measured for absorption spectroscopy to examine the presence of released drug in the collected suspension.

***In Vitro* Biocompatibility.** Various components of carbanosilica such as GQDs and surfactant free silica were selected to examine the biocompatibility of designed carbanosilica at 10−200 μg/mL concentration range. Normal L929 cells were seeded at a density of 1 × 10^5 cells per well in 96 well plates and incubated for 24 h in 5% CO_2 atmosphere at 37 °C using Dulbecco's Modified Eagle's Medium (DMEM Gibco, Carlsbad, CA, USA) supplemented with 10% fetal bovine serum. For MTT assay, after 24 h incubation time, 100 μL of different concentrations (10−200 μg/mL) of carbanosilica, GQDs, and surfactant free silica was added into the wells. After 24 h of incubation, the wells were washed off with PBS and 20 μL of MTT dye was added and formed formazan crystals after 4 h were dissolved using 200 μL of DMSO. Optical absorbance was recorded at 570 and 690 nm using a microplate reader (Tecan Infinite 200 PRO). Percentage cell viability was calculated in reference to untreated cells.

***In Vitro* Cellular Uptake.** 4T1 cancer cells (1 × 10^5) were cultured in DMEM culture media that was supplemented with 10% fetal bovine serum and incubated for 24 h in 5% CO_2 atmosphere at 37 °C. After being rinsed with PBS, 200 μg/mL of carbanosilica nanoparticles were added and incubated for 6 h. After 6 h incubation, cells were washed with PBS three times to get rid of all the unbound particles and 4% paraformaldehyde solution was added to the cells followed by 10 min nuclei staining with 4,6-diamidino-2-phenylindole (DAPI, 1 μg/mL in PBS). After the complete incubation period, the staining solution was repetitively washed with PBS. The coverslip was mounted on a drop of 70% glycerol on a glass slide, and fluorescence images were taken using a fluorescence microscope.

NIR Light Triggered Combined Therapeutic Assessment. 4T1 breast cancer cells were seeded into 96 well plates at a density of 1 × 10^5 cells/well followed by overnight incubation in 5% CO_2 atmosphere at 37 °C. After rinsing the wells with PBS, cells were incubated with 200 μg/mL concentration of surfactant free silica, carbanosilica, and doxorubicin drug loaded carbanosilica nanohybrid each with and without NIR light (800 nm, 1 W/cm^2 power) treatment. After 6 h of incubation, wells were rinsed with PBS three times to get rid of all the unbound particles. After treatment, these plates were incubated for another 15 h. Formed formazan crystals were dissolved by using 200 μL of DMSO. Optical absorbance was recorded at 570 and 690 nm using a microplate reader. Percentage cell viability was calculated in reference to untreated cells. The following groups were considered for comparative therapeutic assessment: only cancer cells, NIR light treated cancer cells, surfactant free silica treated cells with and without 5 min of 800 nm NIR exposure, carbanosilica treated cells with and without 5 min of NIR exposure, and doxorubicin drug loaded carbanosilica treated cancer cells with and without 5 min of NIR exposure. MTT assay was performed to measure the cell viability.

Ethical Approval and Localized Tumor Diagnosis. Protocols for animal experiments (studies with female Balb/c mice) were approved by the Institutional Animal Ethical Committee (IAEC) of National Centre for Cell Science, Pune, India (NCCS, Pune) followed with the IAEC guidelines throughout animal studies. 1 × 10^5 4T1 breast cancer cells were injected subcutaneously into the mammary fat pad of Balb/c mice, and after a week of time tumor growth was measured to begin the further studies.

A single dose (20 mg) of fabricated carbanosilica was administrated on the 4T1 tumor site through an intratumoral route. The fluorescence images of the postinjected tumor bearing Balb/c mice were captured at various time points using an *in vivo* imaging system (IVIS spectrum Xenogen for NIR fluorescence) followed by 530 nm of excitation wavelength. During *in vivo* imaging all animals were anaesthetized. Three mice/group were used for time dependent tumor diagnosis, and five mice/group were prepared to examine the therapeutic outcomes.

Image Guided Tumor Regression Follow-up and Synergistic Phototriggered Chemotherapy. A 20 mg dose of drug loaded carbanosilica nanohybrid was intratumorally injected at the 4T1 tumor site in female Balb/c mice. Postinjected mice were exposed for 5 min of

https://dx.doi.org/10.1021/acsabm.0c01478
ACS Appl. Bio Mater. 2021, 4, 1693−1703

NIR light (800 nm, 1 W/cm^2); then the *in vivo* NIR fluorescence (NIRF) images of treated animals were noted and further followed with fluorescent measurements at various time points (0.5 h, 1 h, 6 h, 24 h, 48 h, 72 h, 6th day, 8th day, and 10th day of postinjection) with anesthetized condition of animals. The qualitative and quantitative measurements for successive tumor regression were made by using NIRF imaging analysis followed by IVIS spectrum Xenogen for NIR fluorescence. Additionally, the temperature measurements from the postinjected tumor site after NIR light irradiation were recorded using a digital thermometer at various time points as mentioned above. Treated mice were compared with the pretreated and preinjected mice group (control).

Next, *in vivo* therapeutic studies were carried out with postinjected tumor bearing balb/c mice with the following groups (5 mice in each group about 20 g body weight): (1) only tumor bearing mice, (2) single dose of doxorubicin loaded carbanosilica injected tumor bearing mice without NIR light irradiation (measured for chemotherapy), and (3) doxorubicin loaded carbanosilica injected (20 mg of single dose) tumor bearing mice with 5 min of 800 nm NIR light exposure (measured for phototriggered chemotherapy). These treatment groups were repeated with an alternative day interval using the above-mentioned conditions. Tumor growth (size and volume) was monitored during 18 days of treatment course. All involved mice in treatment course were sacrificed on the last treatment day to collect tumors for weight measurements. Further, the tumor regression was evaluated by using bioluminescence (using luciferin) observations of treated mice that were compared with preinjected mice (control group).

***In Vivo* Biocompatibility Measurements.** Body weight, health behavior, and histopathological measurements of treated animals were demonstrated to ensure the biocompatibility of injected carbanosilica nanohybrids. Body weight and health measurements of all animals (treated and untreated mice) were regularly noted during the 18 days of treatment planning course. On the 18th day of treatment with respect to the initial cell culture day, animals were sacrificed, and major organs were collected for histopathological studies. During the treatment course the maintained body weight and good health of mice were observed.

Statistics. All experiments for this present work were demonstrated in triplicate and analyzed by Student's *t* test. Spectra, patterns, and graphs were plotted by using OriginPro 8 and sigma plot 10.0 software. Remarkable observations between different groups were assessed by Student's *t* test.

■ ASSOCIATED CONTENT

Supporting Information

The Supporting Information is available free of charge at https://pubs.acs.org/doi/10.1021/acsabm.0c01478.

TEM images measurements, digital photographs, XRD, EDAX, BET, drug loading graph, photoluminescence spectra, cellular uptake images, and *in vitro* and *in vivo* photothermal transduction measurements at various time points, digital photographs of NIR light mediated phototriggered therapy on mice with tumor regression, histopathological images and observations, IVIS image and photograph of major organs, cartoons. (PDF)

■ AUTHOR INFORMATION

Corresponding Authors

Rajendra Prasad − *Department of Biosciences and Bioengineering, Indian Institute of Technology Bombay, Powai, Mumbai, Maharashtra 400076, India;* orcid.org/0000-0001-9851-8630; Email: rpmeena@iitb.ac.in

João Conde − *NOVA Medical School, Faculdade de Ciências Médicas and Centre for Toxicogenomics and Human Health, Genetics, Oncology and Human Toxicology, NOVA Medical School, Faculdade de Ciências Médicas, Universidade Nova de Lisboa, 1169-056 Lisboa, Portugal;* orcid.org/0000-0001-8422-6792; Email: joao.conde@nms.unl.pt

Rohit Srivastava − *Department of Biosciences and Bioengineering, Indian Institute of Technology Bombay, Powai, Mumbai, Maharashtra 400076, India;* orcid.org/0000-0002-3937-5139; Email: rsrivasta@iitb.ac.in

Authors

Nishant K. Jain − *Department of Biosciences and Bioengineering, Indian Institute of Technology Bombay, Powai, Mumbai, Maharashtra 400076, India;* orcid.org/0000-0002-1957-2581

Amit S. Yadav − *Laboratory of Tumor Biology, Angiogenesis and Nanomedicine Research, National Center for Cell Science, Pune 411008, India; School of Biotechnology and Kalinga Institute of Medical Sciences (KIMS), KIIT Deemed to be University, Institute of Eminence, Bhubaneswar 751 024, India*

Manali Jadhav − *Department of Biosciences and Bioengineering and Center for Research in Nano Technology and Science, Indian Institute of Technology Bombay, Powai, Mumbai, Maharashtra 400076, India*

Nalukurthi Naga Venkata Radharani − *Laboratory of Tumor Biology, Angiogenesis and Nanomedicine Research, National Center for Cell Science, Pune 411008, India*

Mahadeo Gorain − *Laboratory of Tumor Biology, Angiogenesis and Nanomedicine Research, National Center for Cell Science, Pune 411008, India*

Gopal C. Kundu − *Laboratory of Tumor Biology, Angiogenesis and Nanomedicine Research, National Center for Cell Science, Pune 411008, India; School of Biotechnology and Kalinga Institute of Medical Sciences (KIMS), KIIT Deemed to be University, Institute of Eminence, Bhubaneswar 751 024, India*

Complete contact information is available at: https://pubs.acs.org/10.1021/acsabm.0c01478

Author Contributions

#R.P. and N.K.J. contributed equally. R.P., N.K.J., and R.S. designed the project. R.P., N.K.J., and M.J. synthesized and characterized the engineered nanohybrids, M.G., A.S.Y., J.C., N.V.V.R., and G.C.K. performed the *in vitro* and *in vivo* studies. R.P., N.K.J., and J.C. wrote the manuscript. All authors have contributed to the final version of the manuscript and given approval for further process.

Notes

The authors declare no competing financial interest.

■ ACKNOWLEDGMENTS

This work was supported by Department of Biotechnology, Government of India. J.C. acknowledges the European Research Council Starting Grant (ERC-StG-2019-848325). We thank the staff of animal house, NCCS, Pune for supporting us during animal studies. We also thank Mr. Sumit for the discussion and Dr. Mukesh K. Kumawat for providing GQDs.

■ REFERENCES

(1) Thakor, A. S.; Gambhir, S. S. Nanooncology: The Future of Cancer Diagnosis and Therapy. *Ca-Cancer J. Clin.* **2013**, *63* (6), 395−418.

(2) Li, C. A Targeted Approach to Cancer Imaging and Therapy. *Nat. Mater.* **2014**, *13* (2), 110−115.

(3) Cobley, C. M.; Chen, J.; Cho, E. C.; Wang, L. V.; Xia, Y. Gold Nanostructures: A Class of Multifunctional Materials for Biomedical Applications. *Chem. Soc. Rev.* **2011**, *40* (1), 44−56.

(4) Piao, Y.; Burns, A.; Kim, J.; Wiesner, U.; Hyeon, T. Designed Fabrication of Silica-Based Nanostructured Particle Systems for Nanomedicine Applications. *Adv. Funct. Mater.* **2008**, *18*, 3745−3758.
(5) Figueiredo, P.; Bauleth-Ramos, T.; Hirvonen, J.; Sarmento, B.; Santos, H. A. The Emerging Role of Multifunctional Theranostic Materials in Cancer Nanomedicine. In *Handbook of Nanomaterials for Cancer Theranostics*; Elsevier, 2018; pp 1−31.
(6) Youn, Y. S.; Bae, Y. H. Perspectives on the Past, Present, and Future of Cancer Nanomedicine. *Adv. Drug Delivery Rev.* **2018**, *130*, 3−11.
(7) Liu, Z.; Jiang, W.; Nam, J.; Moon, J. J.; Kim, B. Y. S. Immunomodulating Nanomedicine for Cancer Therapy. *Nano Lett.* **2018**, *18* (11), 6655−6659.
(8) Balasubramanian, V.; Liu, Z.; Hirvonen, J.; Santos, H. A. Nanomedicine: Bridging the Knowledge of Different Worlds to Understand the Big Picture of Cancer Nanomedicines (Adv. Healthcare Mater. 1/2018). *Adv. Healthcare Mater.* **2018**, *7* (1), 1870005.
(9) Sun, Q.; Barz, M.; De Geest, B. G.; Diken, M.; Hennink, W. E.; Kiessling, F.; Lammers, T.; Shi, Y. Nanomedicine and Macroscale Materials in Immuno-Oncology. *Chem. Soc. Rev.* **2019**, *48* (1), 351−381.
(10) Li, Z.; Liu, J.; Hu, Y.; Howard, K. A.; Li, Z.; Fan, X.; Chang, M.; Sun, Y.; Besenbacher, F.; Chen, C. Multimodal Imaging-Guided Antitumor Photothermal Therapy and Drug Delivery Using Bismuth Selenide Spherical Sponge. *ACS Nano* **2016**, *10* (10), 9646−9658.
(11) Lin, S.; Wang, Y.; Chen, Z.; Li, L.; Zeng, J.; Dong, Q.; Wang, Y.; Chai, Z. Biomineralized Enzyme-Like Cobalt Sulfide Nanodots for Synergetic Phototherapy with Tumor Multimodal Imaging Navigation. *ACS Sustainable Chem. Eng.* **2018**, *6* (9), 12061−12069.
(12) Gai, S.; Yang, G.; Yang, P.; He, F.; Lin, J.; Jin, D.; Xing, B. Recent Advances in Functional Nanomaterials for Light-Triggered Cancer Therapy. *Nano Today* **2018**, *19*, 146−187.
(13) Mehlenbacher, R. D.; Kolbl, R.; Lay, A.; Dionne, J. A. Nanomaterials for in Vivo Imaging of Mechanical Forces and Electrical Fields. *Nat. Rev. Mater.* **2018**, *3* (2), 17080.
(14) Wei, R.; Cai, Z.; Ren, B. W.; Li, A.; Lin, H.; Zhang, K.; Chen, H.; Shan, H.; Ai, H.; Gao, J. Biodegradable and Renal-Clearable Hollow Porous Iron Oxide Nanoboxes for in Vivo Imaging. *Chem. Mater.* **2018**, *30* (21), 7950−7961.
(15) Smith, B. R.; Gambhir, S. S. Nanomaterials for in Vivo Imaging. *Chem. Rev.* **2017**, *117* (3), 901−986.
(16) Prasad, R.; Jain, N. K.; Yadav, A. S.; Chauhan, D. S.; Devrukhkar, J.; Kumawat, M. K.; Shinde, S.; Gorain, M.; Thakor, A. S.; Conde, J.; Srivastava, R. Liposomal Nanotheranostics for Multimode Targeted In Vivo Bioimaging and Near-Infrared Light Mediated Cancer Therapy. *Commun. Biol.* **2020**, *3* (1), 1−14.
(17) Jain, N. K.; Dimri, S.; Prasad, R.; Ravichandran, G.; Naidu, V.; De, A.; Srivastava, R. Characteristics of Molecularly Engineered Anticancer Drug Conjugated Organic Nanomicelles for Site-Selective Cancer Cell Rupture and Growth Inhibition of Tumor Spheroids. *ACS Appl. Bio Mater.* **2020**, *3* (10), 7067−7079.
(18) Prasad, R.; Aiyer, S.; Chauhan, D. S.; Srivastava, R.; Selvaraj, K. Bioresponsive Carbon Nano-Gated Multifunctional Mesoporous Silica for Cancer Theranostics. *Nanoscale* **2016**, *8* (8), 4537−4546.
(19) Huang, X.; Zhang, W.; Guan, G.; Song, G.; Zou, R.; Hu, J. Design and Functionalization of the NIR-Responsive Photothermal Semiconductor Nanomaterials for Cancer Theranostics. *Acc. Chem. Res.* **2017**, *50* (10), 2529−2538.
(20) Lim, E.-K.; Kim, T.; Paik, S.; Haam, S.; Huh, Y.-M.; Lee, K. Nanomaterials for Theranostics: Recent Advances and Future Challenges. *Chem. Rev.* **2015**, *115* (1), 327−394.
(21) Qi, J.; Fang, Y.; Kwok, R. T. K.; Zhang, X.; Hu, X.; Lam, J. W. Y.; Ding, D.; Tang, B. Z. Highly Stable Organic Small Molecular Nanoparticles as an Advanced and Biocompatible Phototheranostic Agent of Tumor in Living Mice. *ACS Nano* **2017**, *11* (7), 7177−7188.
(22) Xie, L.; Wang, G.; Zhou, H.; Zhang, F.; Guo, Z.; Liu, C.; Zhang, X.; Zhu, L. Functional Long Circulating Single Walled Carbon Nanotubes for Fluorescent/Photoacoustic Imaging-Guided Enhanced Phototherapy. *Biomaterials* **2016**, *103*, 219−228.
(23) Li, B.; Wang, X.; Chen, L.; Zhou, Y.; Dang, W.; Chang, J.; Wu, C. Ultrathin Cu-TCPP MOF Nanosheets: A New Theragnostic Nanoplatform with Magnetic Resonance/near-Infrared Thermal Imaging for Synergistic Phototherapy of Cancers. *Theranostics* **2018**, *8* (15), 4086−4096.
(24) Wang, R.; Han, Y.; Sun, B.; Zhao, Z.; Opoku Damoah, Y.; Cheng, H.; Zhang, H.; Zhou, J.; Ding, Y. Deep Tumor Penetrating Bioparticulates Inspired Burst Intracellular Drug Release for Precision Chemo Phototherapy. *Small* **2018**, *14* (12), 1703110.
(25) Yang, X.; Wang, D.; Zhu, J.; Xue, L.; Ou, C.; Wang, W.; Lu, M.; Song, X.; Dong, X. Functional Black Phosphorus Nanosheets for Mitochondria-Targeting Photothermal/Photodynamic Synergistic Cancer Therapy. *Chem. Sci.* **2019**, *10* (13), 3779−3785.
(26) Rastinehad, A. R.; Anastos, H.; Wajswol, E.; Winoker, J. S.; Sfakianos, J. P.; Doppalapudi, S. K.; Carrick, M. R.; Knauer, C. J.; Taouli, B.; Lewis, S. C.; Tewari, A. K. Gold Nanoshell-Localized Photothermal Ablation of Prostate Tumors in a Clinical Pilot Device Study. *Proc. Natl. Acad. Sci. U. S. A.* **2019**, *116* (37), 18590−18596.
(27) Cole, J. R.; Mirin, N. A.; Knight, M. W.; Goodrich, G. P.; Halas, N. J. Photothermal Efficiencies of Nanoshells and Nanorods for Clinical Therapeutic Applications. *J. Phys. Chem. C* **2009**, *113* (28), 12090−12094.
(28) Zhu, S.; Hu, Z.; Tian, R.; Yung, B. C.; Yang, Q.; Zhao, S.; Kiesewetter, D. O.; Niu, G.; Sun, H.; Antaris, A. L. Repurposing Cyanine NIR I Dyes Accelerates Clinical Translation of Near Infrared II (NIR II) Bioimaging. *Adv. Mater.* **2018**, *30* (34), 1802546.
(29) Savani, M.; Murugan, P.; Skubitz, K. M. Long-Term Cure of Soft Tissue Sarcoma with Pegylated-Liposomal Doxorubicin after Doxorubicin and Ifosfamide Failure. *Clin. Sarcoma Res.* **2019**, *9* (1), 1−7.
(30) Hadjidemetriou, M.; McAdam, S.; Garner, G.; Thackeray, C.; Knight, D.; Smith, D.; Al Ahmady, Z.; Mazza, M.; Rogan, J.; Clamp, A. The Human In Vivo Biomolecule Corona onto PEGylated Liposomes: A Proof of Concept Clinical Study. *Adv. Mater.* **2019**, *31* (4), 1803335.
(31) Hori, K.; Ito, K.; Kuritani, K.; Kuji, S.; Furukawa, N.; Tsubamoto, H.; Arakawa, A. *Phase I Study on Pegylated Liposomal Doxorubicin in Combination with Docetaxel for Patients with Platinum-Resistant or Partially Platinum-Sensitive Epithelial Ovarian Cancer: The Kansai Clinical Oncology Group Study* **2019**, *15* (6), 1201−1206.
(32) Ansari, L.; Shiehzadeh, F.; Taherzadeh, Z.; Nikoofal-Sahlabadi, S.; Momtazi-Borojeni, A. A.; Sahebkar, A.; Eslami, S. The Most Prevalent Side Effects of Pegylated Liposomal Doxorubicin Monotherapy in Women with Metastatic Breast Cancer: A Systematic Review of Clinical Trials. *Cancer Gene Ther.* **2017**, *24* (5), 189−193.
(33) Lal, S.; Clare, S. E.; Halas, N. J. Nanoshell-Enabled Photothermal Cancer Therapy: Impending Clinical Impact. *Acc. Chem. Res.* **2008**, *41* (12), 1842−1851.
(34) Chen, F.; Ma, K.; Benezra, M.; Zhang, L.; Cheal, S. M.; Phillips, E.; Yoo, B.; Pauliah, M.; Overholtzer, M.; Zanzonico, P. Cancer-Targeting Ultrasmall Silica Nanoparticles for Clinical Translation: Physicochemical Structure and Biological Property Correlations. *Chem. Mater.* **2017**, *29* (20), 8766−8779.
(35) Bradbury, M. S.; Pauliah, M.; Zanzonico, P.; Wiesner, U.; Patel, S. Intraoperative Mapping of Sentinel Lymph Node Metastases Using a Clinically Translated Ultrasmall Silica Nanoparticle. *Wiley Interdiscip. Rev. Nanomedicine Nanobiotechnology* **2016**, *8* (4), 535−553.
(36) Anselmo, A. C.; Mitragotri, S. A Review of Clinical Translation of Inorganic Nanoparticles. *AAPS J.* **2015**, *17* (5), 1041−1054.
(37) Bobo, D.; Robinson, K. J.; Islam, J.; Thurecht, K. J.; Corrie, S. R. Nanoparticle-Based Medicines: A Review of FDA-Approved Materials and Clinical Trials to Date. *Pharm. Res.* **2016**, *33* (10), 2373−2387.
(38) Anselmo, A. C.; Mitragotri, S. Nanoparticles in the Clinic. *Bioeng. Transl. Med.* **2016**, *1* (1), 10−29.
(39) Arami, H.; Patel, C. B.; Madsen, S. J.; Dickinson, P. J.; Davis, R. M.; Zeng, Y.; Sturges, B. K.; Woolard, K. D.; Habte, F. G.; Akin, D. Nanomedicine for Spontaneous Brain Tumors: A Companion Clinical Trial. *ACS Nano* **2019**, *13* (3), 2858−2869.
(40) Carr, J. A.; Franke, D.; Caram, J. R.; Perkinson, C. F.; Saif, M.; Askoxylakis, V.; Datta, M.; Fukumura, D.; Jain, R. K.; Bawendi, M. G.; Bruns, O. T. Shortwave Infrared Fluorescence Imaging with the

https://dx.doi.org/10.1021/acsabm.0c01478
ACS Appl. Bio Mater. 2021, 4, 1693−1703

Clinically Approved Near-Infrared Dye Indocyanine Green. *Proc. Natl. Acad. Sci. U. S. A.* **2018**, *115* (17), 4465−4470.
(41) Caracciolo, G. Clinically Approved Liposomal Nanomedicines: Lessons Learned from the Biomolecular Corona. *Nanoscale* **2018**, *10* (9), 4167−4172.
(42) Li, T.; Shi, S.; Goel, S.; Shen, X.; Xie, X.; Chen, Z.; Zhang, H.; Li, S.; Qin, X.; Yang, H. Recent Advancements in Mesoporous Silica Nanoparticles towards Therapeutic Applications for Cancer. *Acta Biomater.* **2019**, *89*, 1−13.
(43) Altay, Y.; Cao, S.; Che, H.; Abdelmohsen, L. K. E. A.; van Hest, J. C. M. Adaptive Polymeric Assemblies for Applications in Biomimicry and Nanomedicine. *Biomacromolecules* **2019**, *20* (11), 4053−4064.
(44) Chen, X.; Zheng, G.; Cheng, J.; Yang, Y.-Y. Supramolecular Nanotheranostics. *Theranostics* **2019**, *9* (11), 3014−3016.
(45) Wu, Z.; Song, N.; Menz, R.; Pingali, B.; Yang, Y.-W.; Zheng, Y. Nanoparticles Functionalized with Supramolecular Host-Guest Systems for Nanomedicine and Healthcare. *Nanomedicine* **2015**, *10* (9), 1493−1514.
(46) Yang, K.; Feng, L.; Liu, Z. Stimuli Responsive Drug Delivery Systems Based on Nano-Graphene for Cancer Therapy. *Adv. Drug Delivery Rev.* **2016**, *105*, 228−241.
(47) Zhou, Y.; Jing, X.; Chen, Y. Material Chemistry of Graphene Oxide-Based Nanocomposites for Theranostic Nanomedicine. *J. Mater. Chem. B* **2017**, *5* (32), 6451−6470.
(48) Kostarelos, K. Translating Graphene and 2D Materials into Medicine. *Nat. Rev. Mater.* **2016**, *1*, 16084.
(49) Navalon, S.; Dhakshinamoorthy, A.; Alvaro, M.; Antonietti, M.; Garcia, H. Active Sites on Graphene-Based Materials as Metal-Free Catalysts. *Chem. Soc. Rev.* **2017**, *46* (15), 4501−4529.
(50) Croissant, J. G.; Fatieiev, Y.; Khashab, N. M. Degradability and Clearance of Silicon, Organosilica, Silsesquioxane, Silica Mixed Oxide, and Mesoporous Silica Nanoparticles. *Adv. Mater.* **2017**, *29* (9), 1604634.
(51) Baghirov, H.; Karaman, D.; Viitala, T.; Duchanoy, A.; Lou, Y.-R.; Mamaeva, V.; Pryazhnikov, E.; Khiroug, L.; de Lange Davies, C.; Sahlgren, C. Feasibility Study of the Permeability and Uptake of Mesoporous Silica Nanoparticles across the Blood-Brain Barrier. *PLoS One* **2016**, *11* (8), No. e0160705.
(52) Kolosnjaj-Tabi, J.; Volatron, J.; Gazeau, F. Basic Principles of In Vivo Distribution, Toxicity, and Degradation of Prospective Inorganic Nanoparticles for Imaging. In *Design and Applications of Nanoparticles in Biomedical Imaging*; Springer, 2017; pp 9−41.
(53) Prasad, R.; Agawane, S. B.; Chauhan, D. S.; Srivastava, R.; Selvaraj, K. In Vivo Examination of Folic Acid-Conjugated Gold-Silica Nanohybrids as Contrast Agents for Localized Tumor Diagnosis and Biodistribution. *Bioconjugate Chem.* **2018**, *29* (12), 4012−4019.
(54) Nanda, S.; Antunes, J. T.; Selvam, A.; Bera, K.; Brady, J. T.; Gollamudi, J.; Friedman, K.; Willis, J. E.; Delaney, C. P.; Paspulati, R. M. Integrating Radiomic Features from T2-Weighted and Contrast-Enhanced MRI to Evaluate Pathologic Rectal Tumor Regression after Chemoradiation. In *Medical Imaging 2019: Image-Guided Procedures, Robotic Interventions, and Modeling*; International Society for Optics and Photonics; 2019; Vol. *10951*, p 109512R.
(55) Liu, Y.; Bhattarai, P.; Dai, Z.; Chen, X. Photothermal Therapy and Photoacoustic Imaging via Nanotheranostics in Fighting Cancer. *Chem. Soc. Rev.* **2019**, *48* (7), 2053−2108.
(56) Lu, N.; Fan, W.; Yi, X.; Wang, S.; Wang, Z.; Tian, R.; Jacobson, O.; Liu, Y.; Yung, B. C.; Zhang, G. Biodegradable Hollow Mesoporous Organosilica Nanotheranostics for Mild Hyperthermia-Induced Bubble-Enhanced Oxygen-Sensitized Radiotherapy. *ACS Nano* **2018**, *12* (2), 1580−1591.
(57) Yang, Z.; Dai, Y.; Shan, L.; Shen, Z.; Wang, Z.; Yung, B. C.; Jacobson, O.; Liu, Y.; Tang, W.; Wang, S. Tumour Microenvironment-Responsive Semiconducting Polymer-Based Self-Assembling Nanotheranostics. *Nanoscale Horizons* **2019**, *4* (2), 426−433.
(58) Fan, W.; Yung, B.; Huang, P.; Chen, X. Nanotechnology for Multimodal Synergistic Cancer Therapy. *Chem. Rev.* **2017**, *117* (22), 13566−13638.
(59) Zhan, C.; Wang, W.; McAlvin, J. B.; Guo, S.; Timko, B. P.; Santamaria, C.; Kohane, D. S. Phototriggered Local Anesthesia. *Nano Lett.* **2016**, *16* (1), 177−181.
(60) Prasad, R.; Yadav, A. S.; Gorain, M.; Chauhan, D. S.; Kundu, G. C.; Srivastava, R.; Selvaraj, K. Graphene Oxide Supported Liposomes as Red Emissive Theranostics for Phototriggered Tissue Visualization and Tumor Regression. *ACS Appl. Bio Mater.* **2019**, *2* (8), 3312−3320.
(61) Prasad, R.; Chauhan, D. S.; Yadav, A. S.; Devrukhkar, J.; Singh, B.; Gorain, M.; Temgire, M.; Bellare, J.; Kundu, G. C.; Srivastava, R. A Biodegradable Fluorescent Nanohybrid for Photo-Driven Tumor Diagnosis and Tumor Growth Inhibition. *Nanoscale* **2018**, *10* (40), 19082−19091.
(62) Nurunnabi, M.; Khatun, Z.; Huh, K. M.; Park, S. Y.; Lee, D. Y.; Cho, K. J.; Lee, Y. In Vivo Biodistribution and Toxicology of Carboxylated Graphene Quantum Dots. *ACS Nano* **2013**, *7* (8), 6858−6867.
(63) Geng, B.; Yang, D.; Pan, D.; Wang, L.; Zheng, F.; Shen, W.; Zhang, C.; Li, X. NIR-Responsive Carbon Dots for Efficient Photothermal Cancer Therapy at Low Power Densities. *Carbon* **2018**, *134*, 153−162.
(64) Yao, X.; Tian, Z.; Liu, J.; Zhu, Y.; Hanagata, N. Mesoporous Silica Nanoparticles Capped with Graphene Quantum Dots for Potential Chemo-Photothermal Synergistic Cancer Therapy. *Langmuir* **2017**, *33* (2), 591−599.
(65) Fang, J.; Liu, Y.; Chen, Y.; Ouyang, D.; Yang, G.; Yu, T. Graphene Quantum Dots-Gated Hollow Mesoporous Carbon Nanoplatform for Targeting Drug Delivery and Synergistic Chemo-Photothermal Therapy. *Int. J. Nanomed.* **2018**, *13*, 5991−6007.
(66) Kumawat, M. K.; Srivastava, R.; Thakur, M.; Gurung, R. B. Graphene Quantum Dots from Mangifera Indica: Application in near-Infrared Bioimaging and Intracellular Nanothermometry. *ACS Sustainable Chem. Eng.* **2017**, *5* (2), 1382−1391.
(67) Qian, M.; Chen, L.; Du, Y.; Jiang, H.; Huo, T.; Yang, Y.; Guo, W.; Wang, Y.; Huang, R. Biodegradable Mesoporous Silica Achieved via Carbon Nanodots-Incorporated Framework Swelling for Debris-Mediated Photothermal Synergistic Immunotherapy. *Nano Lett.* **2019**, *19* (12), 8409−8417.
(68) Zhang, X.; Xi, Z.; Machuki, J. O.; Luo, J.; Yang, D.; Li, J.; Cai, W.; Yang, Y.; Zhang, L.; Tian, J. Gold Cube-in-Cube Based Oxygen Nanogenerator: A Theranostic Nanoplatform for Modulating Tumor Microenvironment for Precise Chemo-Phototherapy and Multimodal Imaging. *ACS Nano* **2019**, *13* (5), 5306−5325.
(69) Yao, Y.; Zhao, D.; Li, N.; Shen, F.; Machuki, J. O.; Yang, D.; Li, J.; Tang, D.; Yu, Y.; Tian, J. Multifunctional Fe3O4@ Polydopamine@ DNA-Fueled Molecular Machine for Magnetically Targeted Intracellular Zn2+ Imaging and Fluorescence/MRI Guided Photodynamic-Photothermal Therapy. *Anal. Chem.* **2019**, *91* (12), 7850−7857.
(70) Zhang, X.; Ong'achwa Machuki, J.; Pan, W.; Cai, W.; Xi, Z.; Shen, F.; Zhang, L.; Yang, Y.; Gao, F.; Guan, M. Carbon Nitride Hollow Theranostic Nanoregulators Executing Laser-Activatable Water Splitting for Enhanced Ultrasound/Fluorescence Imaging and Cooperative Phototherapy. *ACS Nano* **2020**, *14* (4), 4045−4060.
(71) Zhu, H.; Wang, Y.; Chen, C.; Ma, M.; Zeng, J.; Li, S.; Xia, Y.; Gao, M. Monodisperse Dual Plasmonic Au@ Cu2-x E (E= S, Se) Core@ Shell Supraparticles: Aqueous Fabrication, Multimodal Imaging, and Tumor Therapy at in Vivo Level. *ACS Nano* **2017**, *11* (8), 8273−8281.
(72) Zhang, H.; Li, Y.; Pan, Z.; Chen, Y.; Fan, Z.; Tian, H.; Zhou, S.; Zhang, Y.; Shang, J.; Jiang, B. Multifunctional Nanosystem Based on Graphene Oxide for Synergistic Multistage Tumor-Targeting and Combined Chemo-Photothermal Therapy. *Mol. Pharmaceutics* **2019**, *16* (5), 1982−1998.
(73) Wang, Y.; Wang, F.; Shen, Y.; He, Q.; Guo, S. Tumor-Specific Disintegratable Nanohybrids Containing Ultrasmall Inorganic Nanoparticles: From Design and Improved Properties to Cancer Applications. *Mater. Horiz.* **2018**, *5* (2), 184−205.

https://dx.doi.org/10.1021/acsabm.0c01478
ACS Appl. Bio Mater. 2021, 4, 1693−1703